

Closed-Loop Measurements of Iso-Response Stimuli Reveal Dynamic Nonlinear Stimulus Integration in the Retina

Daniel Bölinger^{1,2} and Tim Gollisch^{1,2,3,4,*}

¹Max Planck Institute of Neurobiology, Visual Coding Group, 82152 Martinsried, Germany

²Bernstein Center for Computational Neuroscience Munich, 82152 Martinsried, Germany

³Department of Ophthalmology, University Medical Center Göttingen, 37073 Göttingen, Germany

⁴Bernstein Center for Computational Neuroscience Göttingen, 37073 Göttingen, Germany

*Correspondence: tim.gollisch@med.uni-goettingen.de

DOI 10.1016/j.neuron.2011.10.039

SUMMARY

Neurons often integrate information from multiple parallel signaling streams. How a neuron combines these inputs largely determines its computational role in signal processing. Experimental assessment of neuronal signal integration, however, is often confounded by cell-intrinsic nonlinear processes that arise after signal integration has taken place. To overcome this problem and determine how ganglion cells in the salamander retina integrate visual contrast over space, we used automated online analysis of recorded spike trains and closed-loop control of the visual stimuli to identify different stimulus patterns that give the same neuronal response. These iso-response stimuli revealed a threshold-quadratic transformation as a fundamental nonlinearity within the receptive field center. Moreover, for a subset of ganglion cells, the method revealed an additional dynamic nonlinearity that renders these cells particularly sensitive to spatially homogeneous stimuli. This function is shown to arise from a local inhibition-mediated dynamic gain control mechanism.

INTRODUCTION

A fundamental building block of neuronal circuits is the convergence of parallel streams of information onto single neurons. How a neuron combines these inputs into an output of its own shapes the computation that is performed by the circuit. Obtaining a functional description of how incoming signals are pooled is therefore a crucial step for understanding neuronal information processing. Here, we study the rules of signal integration in retinal ganglion cells and ask how these cells combine stimulus components from different locations within their receptive field centers.

In the retina, research on spatial integration of visual stimuli has focused on distinguishing linear and nonlinear integration

by X-type and Y-type ganglion cells, respectively (Enroth-Cugell and Robson, 1966; Hochstein and Shapley, 1976). Less is known, on the other hand, about what functional types of nonlinearities determine signal integration in the retina (Schwartz and Rieke, 2011). Parameterized model fits have suggested that Y-cell characteristics result from half-wave rectification in spatial subunits (Hochstein and Shapley, 1976; Victor and Shapley, 1979; Victor, 1988; Baccus et al., 2008). Bipolar cell input into the ganglion cells has been identified as the likely source of this rectification (Demb et al., 2001), and rectified input currents have been directly measured in neurons of the inner retina (Molnar et al., 2009). Yet, detailed quantitative characterizations of the nonlinearities that govern stimulus integration over space are still lacking, despite their importance for establishing specific visual functions that are achieved by different types of retinal ganglion cells (Ölveczky et al., 2003; Gollisch and Meister, 2008; Münch et al., 2009; Gollisch and Meister, 2010).

This calls for methods to directly determine how ganglion cells combine their inputs from different parts of their receptive fields. However, assessments of stimulus integration by simply measuring stimulus-response functions are easily confounded by the presence of additional nonlinear processes. For example, neuronal responses will typically show a nonlinear dependence on stimulus intensity simply because of the spiking nonlinearity, leading to thresholding and saturation of the response. In addition, the neuron's intrinsic ionic conductances can contribute to a nonlinear gain of the membrane potential. These nonlinearities occur after signal integration has taken place and therefore reveal little about signal integration itself.

To overcome these limitations, we here present an approach for measuring signal integration in retinal ganglion cells while avoiding effects of cell-intrinsic nonlinearities. This is achieved by identifying different stimulus patterns that all yield the same neuronal response. These iso-response stimuli reveal whether signal integration happens linearly or otherwise which types of nonlinearities occur (Gollisch et al., 2002; Benda et al., 2007). To efficiently measure iso-response stimuli, we developed a closed-loop experimental design in which extracellularly recorded spike trains are automatically analyzed so that the presented visual stimuli are tuned until the designated response is reached. For retinal ganglion cells in the salamander retina, this

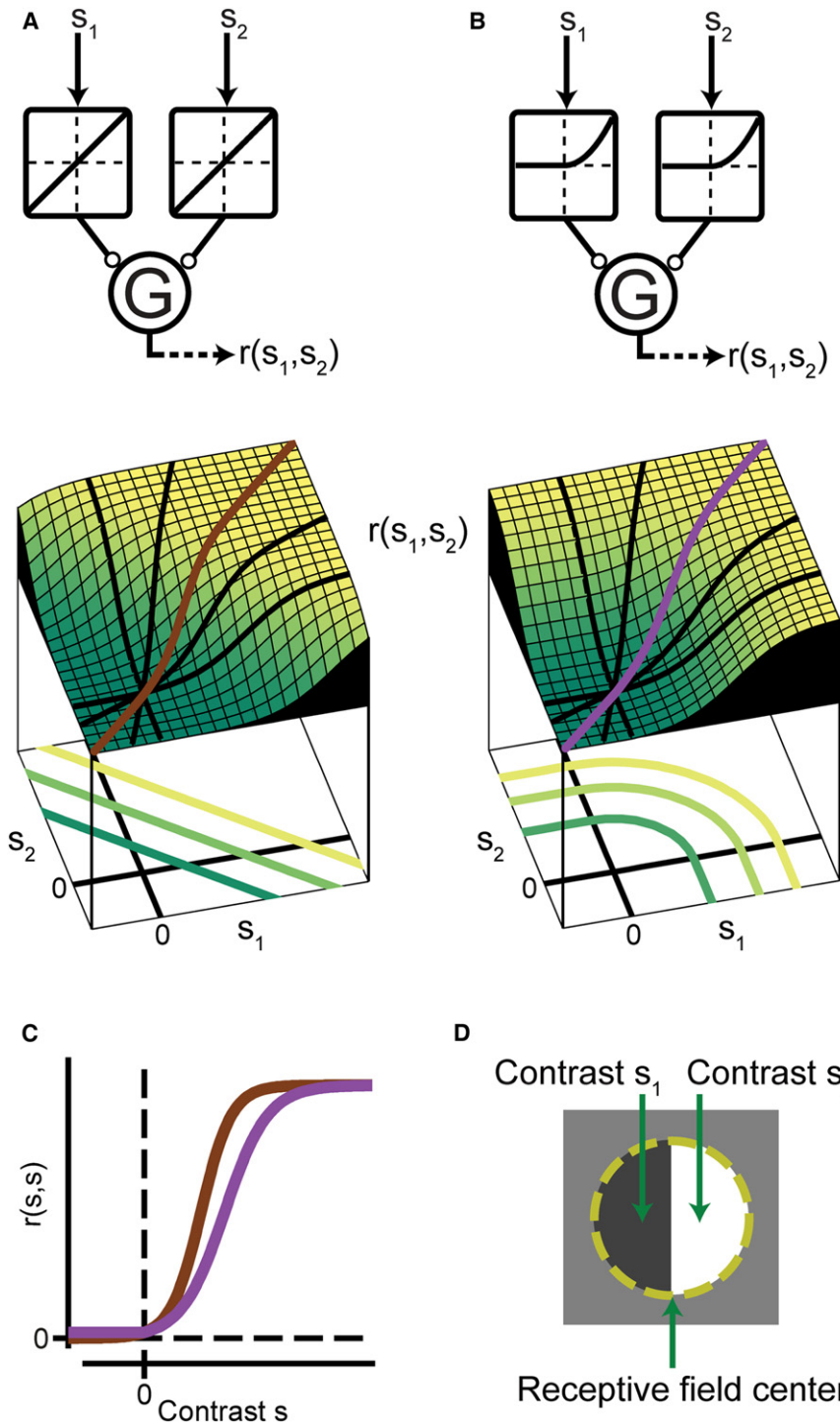


Figure 1. Iso-Response Curves as a Tool for Assessing Stimulus Integration

(A) A subunit model, which takes two inputs s_1 and s_2 and generates a response $r(s_1, s_2)$ (top) and the corresponding two-dimensional stimulus-response plot (bottom). Here, the ganglion cell (G) simply performs a linear summation of the subunit signals. Correspondingly, the iso-response curves, shown below, are straight lines.

(B) Same as (A), but with a subunit model that transforms each subunit input according to a threshold-quadratic nonlinearity. Correspondingly, the iso-response curves now have segments parallel to the axes, representing the threshold operation, and are circular in the central region, representing the summation of squared positive inputs.

(C) Sample stimulus-response curves along a fixed direction in stimulus space, here the direction given by $s_1 = s_2$, for the linear subunit model (brown) and the threshold-quadratic subunit model (purple). The curves are also highlighted in (A) and (B), respectively. The sigmoid shapes of the curves follow from the output nonlinearities of the models.

(D) Stimulus structure for the present study. The two input components s_1 and s_2 correspond to the contrast values displayed in the two halves of a ganglion cell's receptive field center.

objects. The nonlinearity that mediates this function is shown to arise from an inhibition-mediated local gain control mechanism.

RESULTS

Utility of Iso-Response Stimuli

Neurons process information by combining multiple inputs and generating their own output accordingly. As a minimal circuit for neural computation, let us therefore consider a neuron that integrates two input signals (Figure 1). Even if the inputs are simply summed in a linear fashion (Figure 1A), the final response is typically nonlinear because the output neuron contributes its own, intrinsic nonlinear transformation, for example, through a spike generation mechanism that imposes a threshold or response saturation. This nonlinearity may easily appear to dominate the

method revealed that signals are integrated nonlinearly over the receptive field center. The corresponding nonlinearity resembles a threshold-quadratic transformation of the incoming signals. In addition, for a subset of ganglion cells, the method revealed a further nonlinear operation that provides these cells with a particular sensitivity for homogeneous stimulation of the receptive field. These cells are thus especially suited to detect large

stimulus-response function and give it a similar general appearance even for a fundamentally different model of stimulus integration, for example, when inputs are thresholded and squared before pooling (Figure 1B). For both considered models of Figure 1, the response rises with increasing overall stimulus intensity in a sigmoid fashion (Figure 1C), as determined by the intrinsic nonlinearities of each output neuron.

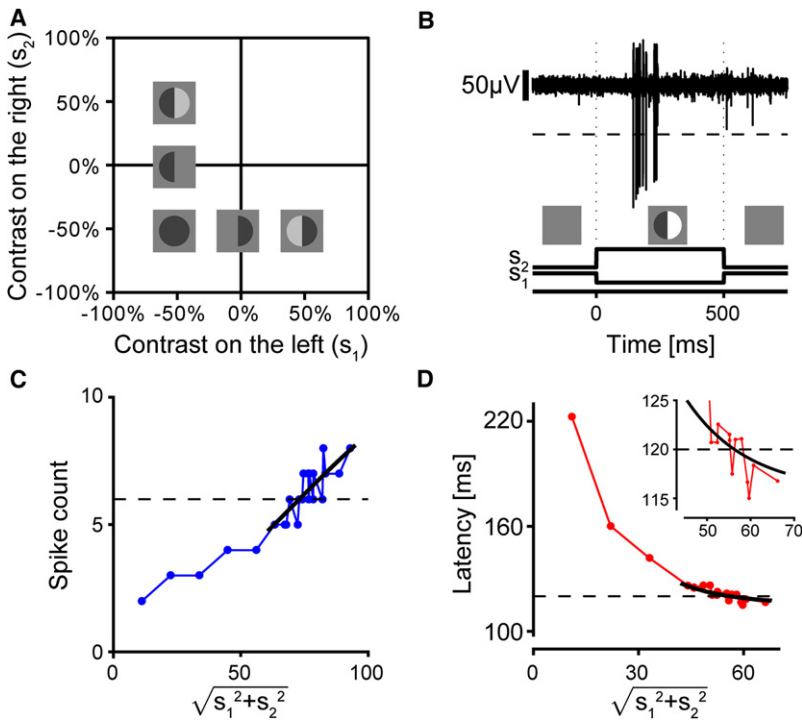


Figure 2. Online Identification of Iso-Response Stimuli

(A) Illustration of stimulus space. The two axes denote the contrast values of s_1 and s_2 , respectively. For positive contrast values, the corresponding stimulus area turns brighter; for negative contrast values, it turns darker, with zero contrast denoting the gray background level. Several sample stimuli are shown at the corresponding locations in the plot. Along the axes, only one half of the receptive field center is stimulated. Along the diagonal toward the lower left, s_1 and s_2 are equal, and the receptive field center is thus stimulated homogeneously. Individual searches were performed in the radial directions of this stimulus space. (B) Voltage trace measured for a single stimulus presentation (top) and corresponding time course of the stimulus (bottom). Spikes were detected as excursions of the voltage trace below a selected threshold (horizontal dashed line). The stimulus here was a 500 ms presentation of negative contrast (dimming) for s_1 and positive contrast (brightening) for s_2 .

(C) Sample data of an individual line search for a predefined spike count. Spike counts were measured for different overall contrast values while keeping a fixed ratio of s_1 and s_2 , corresponding to a fixed radial direction in stimulus space. Data points near the target response were fitted by a straight line (black line). The horizontal dotted line shows the predefined target response, here six spikes. (D) Line search for a predefined first-spike latency, displayed in the same way as (C). Here, the target latency was 120 ms and the data were fitted by an exponential curve (black line). The inset shows a zoom-in of the data close to the target latency.

Despite these similarities in the general shape of the stimulus-response relations, the characteristic differences of stimulus integration in the two models become strikingly apparent when one considers the contour lines of the stimulus-response plot, that is, the lines along which the response of the output neuron stays the same (Figures 1A and 1B, shown below the stimulus-response surface plots). The shape of these iso-response curves is a clear signature of the underlying signal integration or, in other words, of the arithmetic rule with which the output neuron combines its inputs. In the simplest case, linear summation of inputs is reflected by straight lines in the iso-response curves (Figure 1A). The circular part of the iso-response curves in Figure 1B, on the other hand, shows the summation of squared positive inputs, whereas the line segments that run parallel to the axes indicate the thresholding of negative inputs. Iso-response curves thus reveal the nature of stimulus integration independently of the neuron's intrinsic output nonlinearity; the output nonlinearity simply affects the response equally for all stimuli along an iso-response curve and thus does not influence the curve's shape.

To assess the nature of signal integration within the receptive field center of retinal ganglion cells, we developed an approach to measure these iso-response curves. We used a stimulus layout that subdivided the receptive field center of a ganglion cell into two halves and stimulated the cell with different levels of light intensity in these two regions (Figure 1D). Iso-response curves then consisted of those pairs of visual contrast in the two receptive field halves (measured relative to the mean

background light intensity) that yielded a fixed, predefined spike response of the ganglion cell.

Measuring Iso-Response Stimuli

Seeking iso-response stimuli poses an obvious experimental challenge; instead of measuring responses for predefined stimuli, we need to find stimuli for predefined neuronal responses. To achieve this, we devised a closed-loop experimental design to automatically and quickly tune stimulus intensities toward the desired response, similar to previous applications in the auditory system (Gollisch et al., 2002; Gollisch and Herz, 2005). We recorded spiking activity extracellularly from individual ganglion cells in isolated salamander retinas. For every analyzed cell, we first used the online analysis to map out the location and size of the cell's receptive field center. After dividing the receptive field center into two halves, we presented simultaneous short steps in light intensity in both halves on a gray background. Each stimulus was thus defined by a pair of contrast values (Figure 2A).

For each stimulus presentation, a ganglion cell typically responded with a burst of spikes, which were detected automatically with a simple threshold operation (Figure 2B). We first set out to search for combinations of contrasts that elicited the same average spike count in this burst. As the spike count typically provides the basis for calculating a neuron's average firing rate, we refer to these contrast combinations as iso-rate stimuli. As an alternative, we also searched for contrast combinations that resulted in the same average first-spike latency, thus obtaining iso-latency stimuli. We performed individual

searches by fixing the ratio of the two contrast levels and then varying the overall contrast level to perform a simple line search (Figures 2C and 2D). As spike count increased and first-spike latency decreased monotonically for increasing overall contrast in the measured range, the iso-rate and iso-latency stimuli could be reliably identified. This procedure was then performed for several different ratios of the two contrast levels.

Spatial Integration Is Nonlinear

We visualize the obtained iso-response stimuli in the two-dimensional stimulus space that is given by the contrast values in the two receptive field halves (Figure 2A). The vast majority of ganglion cells in the salamander retina are dominated by Off-type responses (Burkhardt et al., 1998; Segev et al., 2006; Geffen et al., 2007), and we therefore focused on Off-type ganglion cells in this work. Figures 3A–3C show measured iso-response curves for three representative ganglion cells. Iso-latency curves (red lines) always looked qualitatively similar. In particular, the curves were approximately parallel to the axes in those regions of stimulus space where one half of the receptive field experienced an increase in light intensity. This means that for a stimulus that contained both “On” and “Off” components in different parts of the receptive field, the strength of the “On” component had virtually no effect on the latency; this component was apparently cut off by a threshold nonlinearity, providing half-wave rectification of the input signal.

In that region of stimulus space where both receptive field halves experienced negative contrast, the iso-latency curves had an approximately circular shape. This indicated that two “Off” components of a stimulus were combined nonlinearly and that the nonlinearity approximately corresponded to a sum of squares. Indeed, we could fit the iso-response curves by a minimal model (Figure 1) where each of the two input signals is transformed by a parameterized nonlinearity (see *Experimental Procedures*) before summation by the ganglion cell. As expected, the obtained nonlinearities generally resembled threshold-quadratic functions (insets in Figures 3A–3C, red lines): nonpreferred signals are half-wave rectified by a threshold, and preferred signals are squared before summation. For some cells, rectification was incomplete, as seen by the shallow, but nonzero slope of the obtained nonlinearities for nonpreferred signals (Figure 3B).

Iso-rate curves (Figures 3A–3C, blue lines) displayed more variable shapes than iso-latency curves. For some cells, the iso-rate curve had approximately the same shape as the cell’s iso-latency curve (Figures 3A and 3B), also indicating a nonlinearity of stimulus integration that is approximately threshold-quadratic or sometimes close to threshold-linear (insets in Figures 3A and 3B, blue lines). For other ganglion cells, however, the iso-rate curves displayed a notably different shape (Figure 3C), characterized by a notch along the lower-left diagonal. This notch gave the curves a distinctive nonconvex shape. It showed that relatively little contrast was required for these cells to achieve the predefined spike count when both receptive field halves were stimulated with similar (negative) contrast. Stimulation of only one receptive field half, on the other hand, required much larger contrast values. Thus, when considering the spike count, these ganglion cells displayed exceptional sensitivity to

spatially homogeneous stimulation of the receptive field, and in the following we will therefore refer to these cells as homogeneity detectors.

The classification of iso-rate curves into convex and nonconvex curves did not depend on the chosen target spike count. Convex iso-rate curves appeared to be largely scaled versions of each other if measured for the same cell at different spike counts (Figure 3D), whereas iso-rate curves of homogeneity detectors displayed the characteristic nonconvex shape over a range of different spike counts (Figure 3E). However, the notch in the iso-rate curve became more pronounced with higher target spike counts, a fact to which we will return when discussing the underlying mechanisms. In addition, the nonconvex shape of homogeneity detectors did not depend on the exact stimulus layout; it proved robust to changes in stimulation radius or insertion of a gap between the two stimulus areas (Figure 3F).

To quantify the degree to which individual iso-response curves were convex or nonconvex, we defined a form factor that compares the radial distance of the curve along the lower-left diagonal to its linear prediction obtained from the intersections of the curve with the two axes of the plot (see *Experimental Procedures* for details). In particular, this form factor is smaller than unity for a nonconvex iso-rate curve as in Figure 3C and larger than unity for the iso-response curves of Figures 3A and 3B. Calculating the form factor for all measured iso-response curves confirmed that iso-latency curves always had similar convex shapes (Figure 3G). In fact, their form factors clustered around their average value of 1.38 (standard deviation: 0.08), close to the value of $\sqrt{2} \approx 1.41$, which is expected from quadratic integration of preferred stimuli. Form factors of iso-rate curves, on the other hand, could be roughly divided into two groups with values larger and smaller than unity, respectively (Figure 3H). This shows that homogeneity detectors were not a rare exception in our recordings; 20 out of 45 measured cells had an iso-rate form factor smaller than unity, indicative of the characteristic nonconvex iso-rate curve. Interestingly, these small iso-rate form factors occurred almost exclusively for cells with large receptive fields (Figure 3I), supporting the idea that homogeneity detectors form a particular subclass of ganglion cells.

Spatial Scale of Nonlinearities

In order to search for the mechanisms underlying the observed nonlinear features of stimulus integration, we first probed the spatial scale at which these occur. To this end, we spatially interleaved the two stimulus components by arranging them in a checkerboard fashion with various sizes of the checkerboard squares. We then measured iso-rate curves for these interleaved stimulus components. We found that stimulus integration generally became linear if the squares were sufficiently small (Figure 4): the thresholding of nonpreferred positive contrasts disappeared (Figure 4A and 4B), and homogeneity detectors lost the nonconvex shape of their iso-rate curves (Figure 4B). These data are consistent with a subunit model (Hochstein and Shapley, 1976; Enroth-Cugell and Freeman, 1987; Victor, 1988; Crook et al., 2008), in which the receptive field is composed of linear subunits whose outputs are nonlinearly combined.

To obtain an estimate of the spatial scale of the subunits, we quantified the amount of rectification depending on the size of

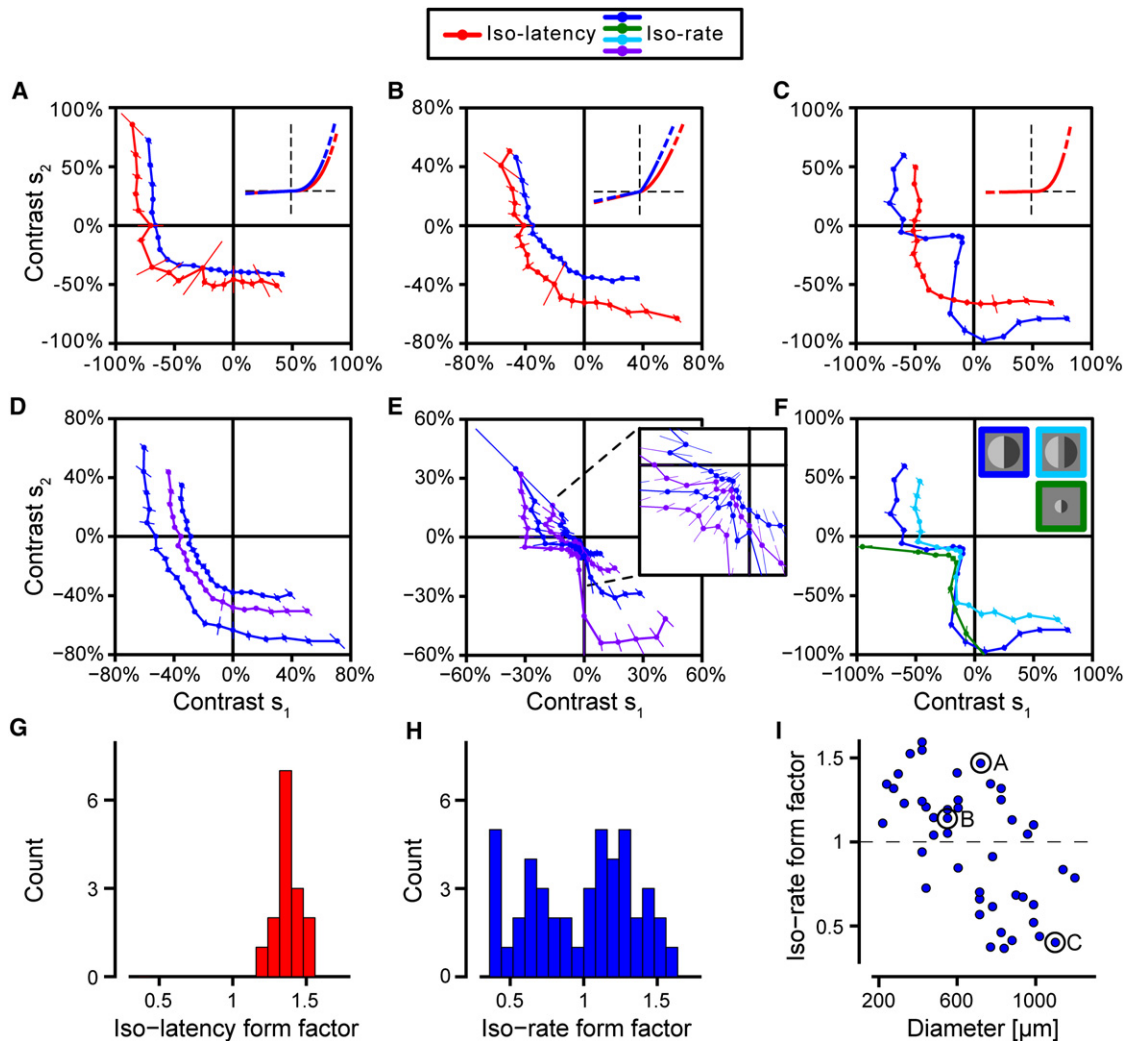


Figure 3. Iso-Response Curves of Retinal Ganglion Cells

(A–C) Iso-rate (blue) and iso-latency curves (red) from three different sample ganglion cells. Here and in subsequent plots, error bars are drawn in the radial direction, corresponding to the direction of measurement, and denote 95% confidence intervals, obtained from fitting the data points of the line searches. Predefined target responses were 6 spikes and 170 ms (A); 4 spikes and 150 ms (B); 8 spikes and 120 ms (C). Insets show the corresponding nonlinearities obtained from a subunit model such as in Figures 1A and 1B. Note that preferred stimuli are displayed as positive values on the x axis of the insets even though they correspond to negative contrast, as these neurons are Off-type ganglion cells. An example with slight deviations from the threshold-quadratic nonlinearity is shown in (B); rectification is incomplete here, and the iso-rate curve yields a rather linear than quadratic summation of negative contrast. For the nonconvex iso-rate curve of (C), no nonlinearity was determined, as the curve is not well described by the static subunit model. Note that the iso-response curves are not always symmetric with respect to the two stimulus components; this results from slight misalignment of the stimulus with the receptive field center and from asymmetries in the receptive field structure.

(D) Iso-rate curves for different target spike counts obtained from a single ganglion cell with convex iso-rate curves. Target spike counts were two, four, and six spikes, in order of increasing distance of the curves from the origin.

(E) Iso-rate curves for different target spike counts obtained from a single homogeneity detector. Target spike counts were three, four, five, and six spikes, in order of increasing distance of the curves from the origin. The inset shows a zoom-in of the central region of the iso-rate curves.

(F) Iso-rate curves from a single homogeneity detector for stimulus layouts with a 100 μm gap between the two stimulation areas (light blue) and for stimulation area with diameter reduced by 60% (green), compared to control condition (dark blue).

(G) Histogram of form factors obtained from iso-latency curves. The values cluster near $\sqrt{2}$, the expected value for convex, circular curves.

(H) Histogram of form factors obtained from iso-rate curves. Values larger and smaller than unity indicate convex and nonconvex iso-rate curves, respectively. Note that the total cell count here is higher than in (G) because iso-latency curves were not measured for all cells.

(I) Scatter plot of form factors from iso-rate curves against receptive field diameter. Small form factors were found almost exclusively for ganglion cells with rather large receptive field centers. The data points corresponding to the cells shown in (A)–(C) are marked by additional black circles.

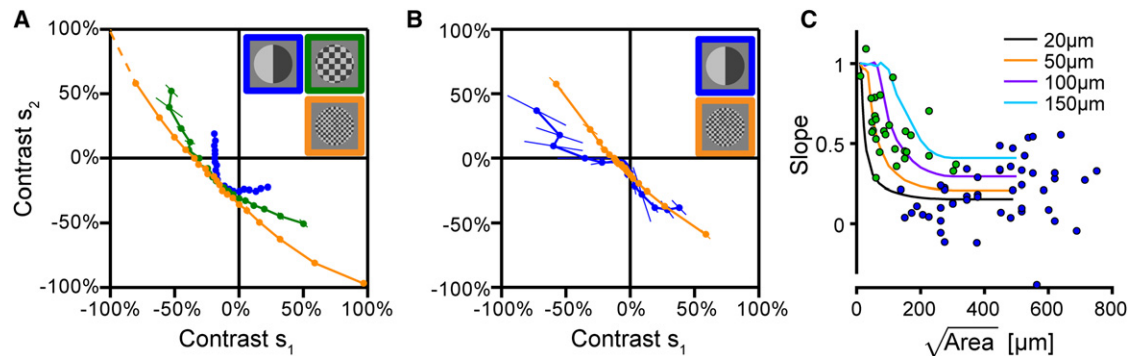


Figure 4. Spatial Scale of Nonlinearities

(A) Iso-rate curves for the control condition (blue) and for two checkerboard arrangements of the two stimulus components with edge length of the squares of 150 μm (green) and 60 μm (orange). Target response: four spikes. Note that stimuli are identical along the diagonal toward the lower left ($s_1 = s_2$) for the three stimulus layouts; correspondingly the three iso-rate curves meet on this diagonal.

(B) Analogous to (A), but for a cell with a nonconvex iso-rate curve under control conditions. Orange curve: checkerboard arrangement with edge length of 75 μm . Target response: six spikes.

(C) Dependence of rectification on spatial scale. We separately fitted the two tail ends of the iso-rates curves by straight lines to determine slope values of s_1 versus $-s_2$ and s_2 versus $-s_1$, respectively. Values of zero and unity correspond to perfect half-wave rectification and to the absence of rectification, respectively. Each data point shows the average of these two slope values for each iso-response curve, plotted against the spatial scale of the stimulus, defined as the square root of the area of the individual stimulus subregions. For data from the checkerboard arrangement (green points), the spatial scale is the edge length of the stimulus squares. The data from control conditions (blue points) serve as providing the baseline. The solid lines show slope values obtained under checkerboard stimulation for a ganglion cell model with spatial subunits of different diameters, ranging from 20 to 150 μm .

the stimulus squares (Figure 4C). The calculated slope values of the tail ends of the iso-rate curves were near unity for small stimulus squares, indicating linear integration, and dropped to a value slightly above zero, indicating strong, though not always complete rectification. The transition roughly occurred over a range up to about 150 μm , suggesting that the spatial scale of subunits is also approximately in this range. For a more quantitative analysis, we compared the experimental data to results of a simple model simulation that uses circular subunits with a rectifying nonlinearity under checkerboard stimulation. From the model, we also calculated the slopes of the iso-rate curves and found that subunits with diameter from about 50 to 100 μm best captured the course of the experimental data (Figure 4C). This spatial scale corresponds well to the typical diameter of bipolar cell receptive fields (Wu et al., 2000; Baccus et al., 2008), making the direct excitatory input from bipolar cells a good candidate for the source of the nonlinearities. Indeed, nonlinear signal transmission from bipolar cells has been suggested to contribute to nonlinearities in ganglion cell receptive fields (Demb et al., 2001; Öveczky et al., 2003; Baccus et al., 2008; Gollisch and Meister, 2008; Molnar et al., 2009) and may thus underlie the threshold-quadratic nonlinearity apparent in the iso-latency curves and in many of the iso-rate curves. Smaller model subunits of 20 μm diameter, which are still larger than typical salamander photoreceptors (Mariani, 1986; Sherry et al., 1998), are not consistent with the experimental data (Figure 4C), indicating that the nonlinearities do not occur on the level of photoreceptor signals.

Spike Patterns along Iso-Response Curves

Although static nonlinear signaling of bipolar cells may underlie the threshold-quadratic nonlinearity, it cannot explain the

striking difference between the shapes of iso-rate and iso-latency curves for homogeneity detectors. To build an intuition for the processes that give rise to this surprising discrepancy, we analyzed the temporal response profiles for different stimuli along the iso-response curves (Figure 5). To do so, we measured iso-response curves and then chose three characteristic points on the curves for repeated measurements of the corresponding stimuli in randomized fashion.

For cells with similar iso-rate and iso-latency curves, we found, as expected, that response patterns had virtually identical temporal structure along iso-rate curves (Figure 5A). For homogeneity detectors, we first consider stimuli that lie along an iso-latency curve (Figure 5B). As a stronger stimulus typically leads to shorter latency (Figure 2D) (Sestokas et al., 1987), the iso-latency condition means that the different stimulus layouts initially were equally effective. Subsequently, however, the activity under stimulation of half the receptive field (Figure 5B, green and orange lines) did not rise as strongly and last as long as for homogeneous stimulation (Figure 5B, black line). Why did the activity not continue in the same way for the two layouts even though the latency suggested them to be equally strong? A plausible interpretation is that spike bursts for stimulation of half the receptive field were affected by a suppression mechanism that became effective shortly after the initial phase of the spike burst.

This view is consistent with the spike patterns along the iso-rate curves (Figure 5C). Here, the stimulation of half the receptive field has to occur at considerably higher contrast to enforce the same spike count. During the initial response part, this higher contrast provides a much more potent stimulus, thus leading to shorter response latencies (Sestokas et al., 1987). The response to homogeneous stimulation, on the other

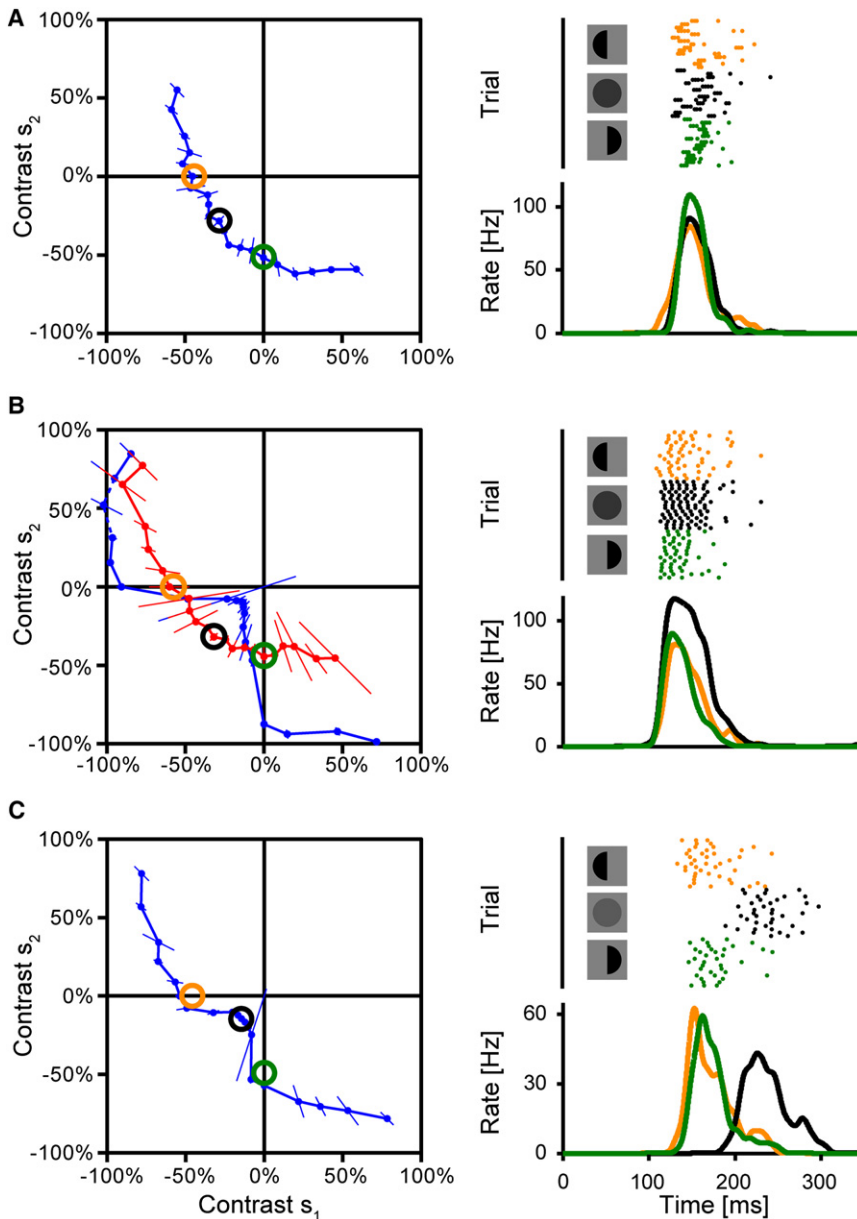


Figure 5. Temporal Response Profile along Iso-Response Curves

(A) Iso-rate curve (left) and spike responses for three selected stimuli (right) of a ganglion cell with a convex iso-rate curve. Open circles along the iso-rate curve denote three stimulus patterns, which were used for repeated measurements. The stimuli correspond to iso-response stimuli on the two axes (stimulation of only one half of the receptive field center) as well as on the lower-left diagonal (homogeneous stimulation of the receptive field center), so that they produced the same spike count on average. The three stimuli were each presented randomly interleaved at least 50 times each. Subsequently, the average spike counts were checked, and the contrast values were adjusted to minimize residual differences in spike counts so that actual applied stimuli might deviate slightly from the original iso-response curve. Raster plots on the right show spikes from 15 repeats of each of the three stimuli. Peristimulus time histograms, shown below, were calculated by convolving the spike patterns with a Gaussian curve of 5 ms standard deviation and averaging over trials.

(B) As (A), but for three iso-latency stimuli of a homogeneity detector with nonconvex iso-rate curve.

(C) As (B) for a second homogeneity detector, but measured for three iso-rate stimuli.

effective and gain stays high. Furthermore, this local gain control can be viewed as a dynamic process; it affects the later part of the spike burst, but not its initial phase, which determines the first-spike latency. In the following, we test neuronal mechanisms that may implement such a dynamic local gain control mechanism.

Mechanisms of Local Gain Control

A first candidate mechanism for local gain control in homogeneity detectors is synaptic depression at bipolar cell terminals. Indeed, bipolar cell signals

can display substantial depression (Burrone and Lagnado, 2000; Singer and Diamond, 2006), which could partly suppress responses to strong local activation. When activation is distributed over more bipolar cells, on the other hand, as in the case of homogeneous receptive field activation, synaptic depression is likely to be less effective and thus should permit longer spike bursts. We therefore tested whether homogeneity detectors are cells with particularly strong local adaptation, as would result from synaptic depression. To do so, we used a stimulus that aimed at predepressing synapses in one half of the receptive field. We assessed the effect of this predepression on the iso-rate curves by a brief activation of one receptive field half shortly before each stimulus of the iso-rate-curve measurement (Figure 6A).

hand, starts later and reaches a smaller peak firing rate, corresponding to the much smaller applied contrast. But it compensates by the slightly longer response duration, presumably due to less suppression, to reach the same average spike count. We thus hypothesize that a suppression mechanism acts on homogeneity detectors for strong local stimulation. Note that local stimulation refers to activation of half the receptive field center in our standard stimulus layout, but strong stimulation in smaller regions also triggers the suppression (Figure 3F). The suppression can be viewed as a local gain control: it reduces the gain when stimulation is strong in a local subregion of the receptive field, corresponding to a strong activation of a subset of available bipolar cells. When stimulation is distributed over all available bipolar cells, but locally weaker, suppression is less

can display substantial depression (Burrone and Lagnado, 2000; Singer and Diamond, 2006), which could partly suppress responses to strong local activation. When activation is distributed over more bipolar cells, on the other hand, as in the case of homogeneous receptive field activation, synaptic depression is likely to be less effective and thus should permit longer spike bursts. We therefore tested whether homogeneity detectors are cells with particularly strong local adaptation, as would result from synaptic depression. To do so, we used a stimulus that aimed at predepressing synapses in one half of the receptive field. We assessed the effect of this predepression on the iso-rate curves by a brief activation of one receptive field half shortly before each stimulus of the iso-rate-curve measurement (Figure 6A).

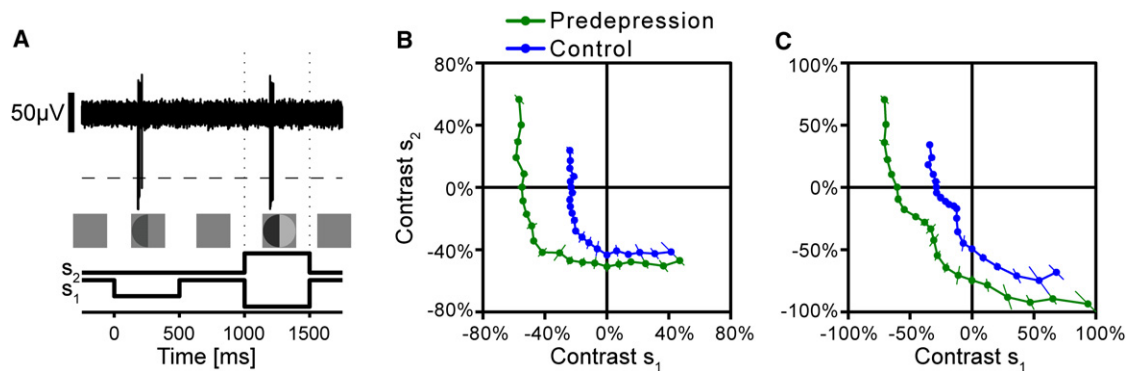


Figure 6. Experimental Test for the Role of Synaptic Depression

(A) Sample recording trace and stimulus layout. The actual iso-response stimulus was preceded by a fixed predepression stimulus (contrast = -40%) presented on one half of the receptive field.

(B) Results for a cell with convex iso-rate curve under control conditions (blue) and in the presence of the predepression stimulus (green). Target response: four spikes.

(C) Same as (B), but for a homogeneity detector with nonconvex iso-rate curve. Target response: six spikes.

As expected, the predepression stimulus reduced sensitivity of the ganglion cells, which is reflected by the increased radius of the iso-rate curves (Figures 6B and 6C) as compared to the control condition without the predepression stimulus. The reduction in sensitivity may contain both global and local components; a symmetric scaling of the predepressed iso-rate-curve radius along all directions reflects a global loss in sensitivity, whereas an asymmetric scaling provides evidence for a local loss in sensitivity and thus a local adaptation mechanism. If the non-convex iso-rate curves of the homogeneity detectors were to result from particularly strong synaptic depression, this asymmetric scaling should be particularly strong for these cells. However, this was not supported by the experimental data. In fact, homogeneity detectors typically displayed rather global adaptation effects and less local sensitivity loss (Figure 6C) than cells with a convex iso-rate curve (Figure 6B). Synaptic depression is thus not a plausible mechanism for the particular features of homogeneity detectors.

As an alternative model, we explored whether local inhibitory signaling could mediate a local gain control. To test the role of inhibition, we pharmacologically blocked all inhibitory synaptic transmission in the retina and then repeated the measurement of the iso-rate curve. The inhibition block had a dramatic effect on the curves (Figure 7A). First, it strongly reduced their radius, corresponding to an overall increase in sensitivity, as expected from the general lack of inhibition. Second, it gave the iso-rate curves of homogeneity detectors a convex shape, similar to the typical iso-response curves of other ganglion cells (Figures 3A and 3B). To quantify this effect, we again computed form factors of the iso-rate curves and found that for all four tested homogeneity detectors, the form factor changed from values below unity in control conditions (range 0.44–0.79) to values above unity under inhibition block (range 1.05–1.60).

The loss of the nonconvex shape of the iso-rate curve is not a result of the reduced contrast level in these inhibition block experiments. When we decreased the radius of the stimulation area in order to reduce the effectiveness of the applied stimuli,

the required contrast levels returned to the range of the control experiment, but the iso-rate curves still remained convex under the inhibition block (Figure 7B). Note that simply reducing the stimulation area without inhibition block did not affect the non-convex shape of the iso-rate curves (Figure 3F). These results suggest that local inhibitory signaling is responsible for the non-convex shape of the iso-rate curves of homogeneity detectors.

This leads us to a simple circuit model for these cells (Figure 7C). They receive excitatory input from bipolar cells, which have smaller receptive fields and therefore constitute the sub-units. The bipolar cell signals undergo a threshold-quadratic nonlinear transformation before they are pooled by the ganglion cell. In addition, the bipolar cells activate local amacrine cells, which provide inhibition either directly to the ganglion cell or as feedback to the bipolar cells. This inhibition operates as the hypothesized dynamic local gain control. To do so, it must come with a temporal delay as compared to the excitatory input to the ganglion cell, and it must have a high threshold or otherwise strongly nonlinear dependence on local stimulus intensity. The temporal delay lets the ganglion cell fire its first spike without the influence of this inhibition so that iso-latency curves simply reflect the fundamental threshold-quadratic nonlinearity of bipolar cell signaling. The strongly nonlinear dependence on stimulus contrast leads to disproportionately larger inhibition when the stimulus is locally strong. This means that, even if the total excitation provided by the bipolar cells is equal for a homogeneous stimulus and for a stimulus that activates only half the receptive field, the latter will incur more inhibition and thus produce fewer spikes. This corresponds to the situation along an iso-latency curve (Figure 5B). Along an iso-rate curve (Figure 5C), the excess inhibition under stimulation of half the receptive field has to be compensated by stronger stimulation, leading to the characteristic nonconvex shape of the iso-response curve.

Indeed, simulating this model circuit reproduces the characteristics of the iso-latency curve as well as of the iso-rate curves with and without inhibition block (Figure 7D). The simulation

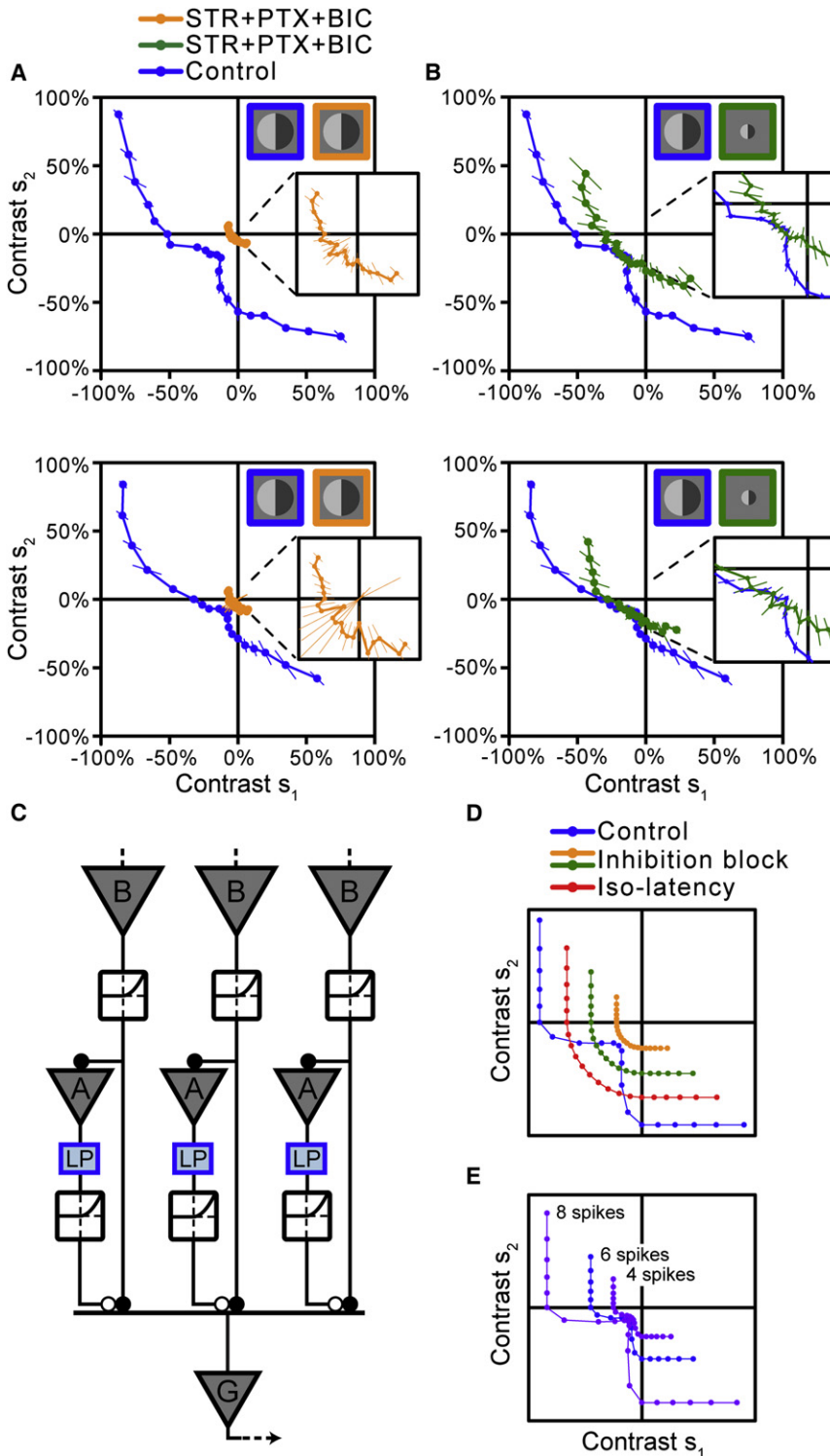


Figure 7. Experimental Test for the Relevance of Inhibition

(A) Iso-rate curves for two different homogeneity detectors under control conditions (blue) and in the presence of a pharmacological block of inhibition (orange). Iso-rate curves became convex when inhibition was removed from the circuit. Target response: six spikes for all curves.

(B) Iso-rate curves for the same cells as in (A), but for stimulation area with diameter reduced by 65% under the inhibition block (green). Target response: six spikes for all curves. Control curves (blue) are the same as in (A).

(C) Circuit model for homogeneity detectors. Bipolar cells (B) are assumed to represent contrast in a linear fashion. Their output undergoes a threshold-quadratic nonlinearity and excites the ganglion cell (G) as well as narrow-field amacrine cells (A). The inhibition provided by the amacrine cells is delayed in time, here through a temporal low-pass filter (LP), and undergoes a further nonlinear transformation, here again of the threshold-quadratic type. The inhibition may act directly on the ganglion cell or on the bipolar cell signal.

(D) Iso-response curves obtained by modeling the circuit shown in (C). The inhibition block was simulated by taking the amacrine cells out of the circuit; the orange curve then shows the obtained iso-rate curve for the standard stimulus layout, the green curve for a stimulus area with diameter reduced by 50%.

(E) Iso-response curves obtained from the model for different target spike counts. For predictions of the same model under stimulation with reversing gratings, see Figure S1.

reaching a higher spike count activates disproportionately more inhibition and thus leads to a stronger gain control effect.

DISCUSSION

Individual neurons typically integrate multiple input components. How they perform this integration is a major factor in determining their computational function. Here, we have suggested to study neuronal integration by measuring iso-response stimuli (Figure 1) and applied this concept to the question how retinal ganglion cells integrate visual stimuli over their receptive field centers. The dominant nonlinearity that was extracted from these measurements was a threshold-quadratic transformation,

which was apparent in all measured iso-latency curves and many iso-rate curves (Figure 3). This nonlinearity occurred on a spatial scale that is consistent with bipolar cell receptive fields (Figure 4). Furthermore, a specific subclass of cells

also shows that the nonconvex shape of the iso-rate curves becomes more pronounced for larger target spike counts (Figure 7E), similar to experimental observations (Figure 3E). This follows because the higher required visual contrast for

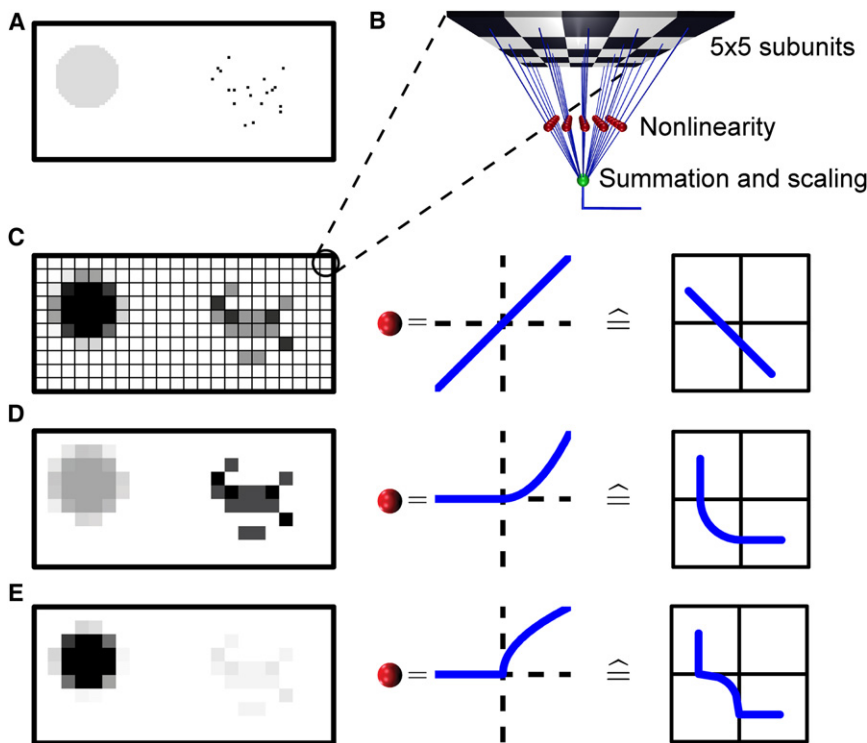


Figure 8. Implications of Spatial Nonlinearities for Image Processing

(A) Sample image, consisting of a large homogeneous low-contrast object and a region with multiple small high-contrast objects.

(B) Model of ganglion cell processing of the image. The image is tiled by the spatial receptive fields of an array of identical ganglion cells. Each ganglion cell's receptive field is divided into a 5×5 matrix of spatial subunits. The subunits are Off-type and linearly integrate the stimulus in their receptive field regions. Their outputs are passed through a nonlinearity and summed by the ganglion cell. In the following image reconstructions, white pixels correspond to a ganglion cell output of zero spikes, and black pixels correspond to the maximum ganglion cell spike count.

(C) Image reconstruction with linear summation of subunit activity (left) and corresponding iso-response curve (right). The grid exemplarily shows the layout of the ganglion cell array; each square corresponds to a receptive field that contains the 5×5 matrix of subunits.

(D) Image reconstruction with a threshold-quadratic nonlinearity applied to the subunit signals (left) and corresponding iso-response curve (right). The region containing small high-contrast objects is amplified.

(E) Image reconstruction with a subunit nonlinearity composed of a threshold and a square-root transformation (left). This nonlinearity can be used

to qualitatively approximate the effect of the nonconvex iso-rate curve observed in homogeneity detectors (right), but it does not aim at capturing the time course of the response, latency effects, or the dependence of iso-rate curves on target spike count (Figure 3E). Now, the region of the homogeneous low-contrast object is amplified.

displayed iso-rate curves that fundamentally differed in shape from the iso-latency curves and were characterized by a particular sensitivity of the spike count for homogeneous stimulation (Figure 3C). For these homogeneity detectors, the difference between iso-latency and iso-rate curves appeared to result from a partial suppression of activity when strong local stimulation in a subregion of the receptive field was involved (Figure 5). This pointed toward a dynamic local gain control mechanism, which was found to be mediated by a local inhibitory circuit (Figure 7), whereas a scenario based on synaptic depression was not consistent with data (Figure 6). The critical role of inhibition for homogeneity detectors further supports the hypothesis of a suppressive mechanism that acts on the spike burst for strong local stimulation. Alternative schemes in which responses might be actively boosted under homogeneous stimulation seem less congruent with a mechanism based on inhibition.

Iso-Response Measurements Provide a Powerful Tool for Analyzing Stimulus Integration

The measurements of iso-response stimuli proved very suited to identify the details of these nonlinearities in ganglion cell receptive fields. First, it required only measurements of spike times from the ganglion cells. These can be obtained in long and stable extracellular recordings, which allowed for detailed characterizations. Second, these measurements could be performed quite efficiently by using automated online analysis and closed-loop control of the stimulation. A measurement of

a single iso-response curve of the type in Figure 3 required around 15 min, which allowed us to use the obtained results in the same experiment for further investigations, such as the detailed PSTH measurements of Figure 5 or comparisons of iso-response curves under different conditions (Figures 3, 4, 6, and 7). Third, the iso-response measurements can assess nonlinearities of stimulus integration by retinal ganglion cells independent of the cell's intrinsic nonlinear processing. This cell-intrinsic nonlinearity implicates, for example, that it is typically not possible to check for linear summation of inputs by comparing the response for multiple simultaneous stimulus components to the sum of responses for the individual components. Such a measurement would require an accurate model of cell-intrinsic signal processing in order to tease apart the different nonlinearities that ultimately affect the response. Fourth, focusing on a fixed response level naturally keeps the neuron close to a constant adaptation level and thus minimizes confounding adaptation effects, as might result from sporadically driving the neuron at particularly high firing rates.

And fifth, iso-response stimuli seem a natural way for investigating the dimensional reduction that results when neurons integrate several inputs and map these inputs onto a low-dimensional response, such as the neuron's spike count. A fundamental consequence is that different input patterns will be mapped onto the same output. This contributes to establishing invariances, which represent a hallmark of neural computation (Riesenhuber and Poggio, 2000) and underlie complex

recognition and decision tasks. It thus appears appropriate to assess computation at the single-neuron level also by identifying which stimuli are classified as equal. Indeed, measuring iso-response stimuli can provide a new perspective on nonlinear signal integration not apparent in other, standard approaches. For example, a simple model simulation shows that homogeneity detectors look just like typical Y-type cells for contrast-reversing gratings (Figure S1 available online), the classical stimulus to test for nonlinear spatial integration.

A caveat of the closed-loop experiments is that they rely on accurate online detection of the incoming signals, here the ganglion cell spikes. Systematic errors in spike detection could, in principle, lead the search for the predefined response astray. We avoided such pitfalls by selecting only ganglion cells whose spikes were sufficiently large for simple and unambiguous detection through threshold crossing. In addition, we verified the accuracy of the online spike detection by additional in-depth offline analysis of the spike waveforms. The selection of large and reliable spikes, however, may add to a potential recording bias (Olshausen and Field, 2005); ganglion cell types with small cell bodies, for example, might not always create spikes with sufficient size in the extracellular recordings (Towe and Harding, 1970; Olshausen and Field, 2005) to pass our criterion of reliable spike detection and may therefore be underrepresented in our analysis. Thus, the observed frequency of homogeneity detectors, for example, does not necessarily reflect the actual occurrence in the retina.

Mechanisms Underlying the Threshold-Quadratic Nonlinearity

The threshold-quadratic nonlinearity appears to be a general property of signal integration in the recorded ganglion cells and presumably corresponds to the nonlinear processing that had been suggested to underlie several specific visual functions solved by the retina (Ölveczky et al., 2003; Gollisch and Meister, 2008, 2010; Münch et al., 2009). Thresholding has been considered previously to lead to nonlinear receptive fields (Shapley and Victor, 1979; Victor and Shapley, 1979; Demb et al., 2001; Ölveczky et al., 2003; Geffen et al., 2007; Gollisch and Meister, 2008; Münch et al., 2009), though often a threshold-linear operation has been hypothesized, rather than the threshold-quadratic transformation observed in this study. Consistent with these previous findings, the source of this nonlinearity appears to be the bipolar cell input into the ganglion cell; the spatial scale of the nonlinearities fits the receptive field size of bipolar cells (Figure 4), and this type of nonlinearity is not affected by a block of inhibitory neurotransmission (Figure 7). The threshold-quadratic nonlinearity may arise in the voltage response of individual bipolar cells (Burkhardt and Fahey, 1998) or in the synaptic transmission at the bipolar cell terminals (Baccus et al., 2008; Molnar et al., 2009). It is noteworthy that iso-latency curves were more consistent in their shapes and always clearly displayed the quadratic part of the nonlinearity (Figure 3G), whereas iso-rate curves, even for cells that were not classified as homogeneity detectors, sometimes showed a tendency toward more linear integration (Figure 3H, see also Figure 3B for an example). This may be explained by local adaptation, for example, synaptic depression, which somewhat

reduces the efficiency of strong local stimulation during the course of the spike burst. It is further interesting to note that no linearly integrating ganglion cells were observed in our study. This might be a feature of the investigated species; in the cat retina, for example, X-type cells would be predicted to have iso-response curves in the shape of straight lines.

Mechanisms Underlying the Local Gain Control of Homogeneity Detectors

The particular sensitivity to homogeneous illumination of the receptive field in homogeneity detectors appears to arise from inhibitory interactions in the circuit. The nonconvex shape of the iso-rate curves was always abolished by removal of inhibition from the retinal circuitry, including experiments with reduced stimulus area so that different ranges of input into the system were tested. Otherwise, the nonconvex shape proved robust to changes in stimulus layout and overall activation level. Together with the success of the computational inhibition model, this supports a principal role of inhibition for generating the response features of homogeneity detectors. The relevant inhibition must be local in the sense that the considered subregions of the ganglion cell's receptive field can activate this inhibition independently. A possible source is narrow-field amacrine cells (Masland, 2001; Chen et al., 2010). The iso-latency curves were not affected by the inhibitory mechanism that underlies the gain control; iso-latency curves always depicted the standard threshold-quadratic nonlinearity. This can simply be explained by a temporal delay of inhibition, resulting from involvement of an additional synaptic stage as compared to the direct excitation from bipolar cells (Werblin and Dowling, 1969; Roska et al., 2006; Cafaro and Rieke, 2010). Note that the inhibition may act as a direct input into the ganglion cells or indirectly by suppressing or modulating the bipolar cell output; the functional characterizations of the present study do not distinguish between these circuit features.

The inhibition makes strong local stimuli that involve only a subset of available bipolar cells less effective, or in other words, it creates a particular sensitivity for spatially homogeneous stimulation when the activity load is shared between all available bipolar cells with weaker individual activation. The characteristic notch in the iso-rate curves of homogeneity detectors can thus be explained completely by local sensitivity changes without the need to evoke a direct interaction between the subregions of the receptive field. Interestingly, an example for the required strongly nonlinear activation of inhibition has recently been found in paired recordings of certain amacrine cells and their presynaptic bipolar cells (Jarsky et al., 2011). The disproportionately stronger activation of inhibition for stronger stimulation also explains why the iso-rate curve shapes differ for different target spike counts. The effect of inhibition becomes stronger with stronger stimulation, and consequently the notch in the iso-rate curves becomes more pronounced with larger target spike counts (Figure 3E and 7E).

Functional Consequences of Different Nonlinearities for Stimulus Integration

The striking differences between different ganglion cells in the nonlinearities of signal integration raise the question of the

associated visual functions. To illustrate the effects of the observed receptive field nonlinearities, let us therefore consider a simple visual stimulus, which contains a large dim object as well as a group of several small objects at high contrast (Figure 8A). When viewed through linear receptive fields, both the large dim object and the area with the small high-contrast objects appear equally prominent (Figure 8C). Receptive fields that integrate their subunits with a threshold-quadratic nonlinearity, however, emphasize the high-contrast region (Figure 8D), whereas nonlinear integration in the fashion of homogeneity detectors facilitates the detection of the large dim object while being insensitive to high-contrast clutter (Figure 8E).

This suggests that homogeneity detectors contribute particularly to the detection of large objects. In fact, these cells typically had rather large receptive field centers (Figure 3I) and no or only weak receptive field surround—features that had also been described previously for certain ganglion cells of the frog retina, so-called dimming detectors (Ishikane et al., 1999, 2005). Those studies had suggested that these cells detect large approaching objects through synchronized oscillatory activity and thereby trigger the frog's escape response to dark looming objects. It is conceivable that this detection of slowly approaching objects works in concert with the detection of suddenly appearing large objects proposed in the present study, thus mediating detection of large, potentially threatening objects over a wide range of behavioral scenarios by a single ganglion cell type in the amphibian retina. Inhibitory signaling appears to be critical for both mechanisms, and indeed, it was shown that the frog's natural escape behavior to large objects is suppressed when inhibition is blocked in the frog's eyes (Ishikane et al., 2005).

Applicability to Other Parts of the Nervous System

The circuit structure proposed to generate the local gain control of homogeneity detectors (Figure 7C) is not unique to the retina. Similar parallel transmission pathways of excitation and inhibition have also been identified elsewhere in the brain (Porter et al., 2001; Pouille and Scanziani, 2001; Gabernet et al., 2005; Sun et al., 2006; Cruikshank et al., 2007; Strowbridge, 2009; Bellavance et al., 2010). Measuring iso-response stimuli in these systems by stimulating local subcircuits independently could be used to probe their functional roles and the potential implementation of a similar local gain control. Moreover, we suggest that measurements of iso-response stimuli can function as a general tool to identify the rules of signal integration in a wide variety of neural systems wherever different signaling streams converge onto single neurons.

EXPERIMENTAL PROCEDURES

Electrophysiology and Visual Stimulation

Retinas were isolated from dark-adapted adult axolotl salamanders (*Ambystoma mexicanum*; pigmented wild-type) and mounted onto 60 channel multielectrode arrays for extracellular recordings of ganglion cell spiking activity. All experimental procedures were performed in accordance with institutional guidelines of the Max Planck Society. During the recordings, retinas were superfused with oxygenated Ringer's solution at room temperature (20°C–22°C). For experiments with pharmacological inhibition block, strychnine (5 μ M), picrotoxin (150 μ M), and bicuculline (20 μ M) were added to the Ringer's solution. Visual stimuli were displayed by a gamma-corrected

cathode ray tube monitor and focused onto the retina with standard optics. Mean light intensities were in the photopic range, and all stated contrast values correspond to Weber contrast $(I_{\text{stimulus}} - I_{\text{background}}) / I_{\text{background}}$. Ganglion cells were classified as either On-type or Off-type, based on their spike-triggered average obtained from recordings under stimulation with spatially uniform broadband flicker (Chichilnisky, 2001). Details of the recordings and stimulation can be found in Supplemental Experimental Procedures.

Closed-Loop Measurements

Data acquisition was controlled with custom-made software, written in Visual C++. Incoming data were both stored for offline analysis as well as directly processed in an online fashion. After visual inspection of the voltage signals of all available channels, one channel was selected that displayed large, homogeneous spike shapes. For this channel, an amplitude threshold was determined, based on a 1 min recording under stimulation with broadband flickering light intensity, to separate spikes from background noise (Figure 2B). Only units whose spike amplitudes were well separated from the noise and that showed a clear refractory period were used for further investigation. To verify that the simple online spike detection and sorting worked well, we occasionally performed additional offline analysis spike sorting, based on the detailed spike shapes (Pouzat et al., 2002). This confirmed the results obtained directly from the online analysis.

To identify the spatial receptive field of a recorded ganglion cell, we first used online analysis to find the midlines of the receptive field in two orthogonal directions. Each midline was determined by dividing the stimulation area by a separation line and comparing responses from stimulation on each side of the line individually. The separation line was then iteratively adjusted until both sides yielded the same response. Finally, receptive field size was determined with blinking spots centered on the crossing point of the two identified midlines.

To measure an iso-response curve, we first selected a predefined response (either average spike count or average first-spike latency). The response selection typically aimed at requiring around 30%–70% contrast for the predefined response from stimulation of one receptive field half alone. Using this range largely avoided coming too close to the physical limit of 100% contrast along the iso-response curve and at the same time provided enough contrast for reliable spike responses. Each data point of an iso-response curve was then obtained by performing a simple line search along a radial direction in stimulus space. Details about the closed-loop experiments and search algorithms are given in Supplemental Experimental Procedures.

Analysis of Iso-Response Curve Shape

We quantitatively analyzed the shape of the iso-response curves in two ways. To determine the degree to which curves were convex or nonconvex (Figures 3G–3I), we calculated form factors that compare the central region of the iso-response curve to the linear prediction that is obtained from the two intersection points of the curve with the axes. The form factor is larger or smaller than unity, depending on whether the iso-response curve is convex or nonconvex, respectively. To assess the amount of rectification (Figure 4C), we calculated the average slope of each iso-rate curve in the regions where one contrast component was negative and the other positive. The slope values were calculated in such a way that zero corresponds to complete rectification whereas a value of unity corresponds to linear summation of s_1 and s_2 . Details of these quantifications can be found in Supplemental Experimental Procedures.

Modeling

Subunit Nonlinearity

To obtain the nonlinearities for the subunit model (insets in Figures 3A–3C), we calculated the ganglion cell response as a weighted sum of two inputs. The two inputs were generated from the respective stimulus components s_1 and s_2 by the same nonlinear function $N(s_i)$. This function is parameterized as a power law for preferred stimuli with potentially incomplete rectification of nonpreferred stimuli. We determined the parameters of the nonlinear function for individual iso-response curves by a maximum-likelihood fit.

Subunit Size

To investigate the effect of subunit size on rectification in the iso-response curves for stimuli arranged in a checkerboard fashion (Figure 4C), we modeled

a ganglion cell with 600 μm receptive field diameter, composed of circular subunits with varying sizes. Each subunit integrated the visual signal linearly and transmitted the result through a threshold-quadratic nonlinearity with incomplete rectification to the ganglion cell. The ganglion cell's response was computed as a weighted sum over all subunit inputs, with weights determined by a Gaussian curve, centered on the midpoint of the ganglion cell receptive field. These responses were used to compute the slope of the iso-response curve in the same way as for the experimentally measured data.

Homogeneity Detectors with Local Inhibitory Circuitry

To quantitatively test the hypothesized circuit for homogeneity detectors based on local inhibition (Figure 7C), we set up a model with two subunits that correspond to the inputs from each half of the receptive field. Each subunit comprises a bipolar cell and an amacrine cell. The bipolar cell transmits the contrast signal of its respective receptive field half as excitatory input to the homogeneity detector through a threshold-quadratic synaptic nonlinearity. The amacrine cell receives the same excitatory input from the bipolar cell and provides inhibition through another threshold-quadratic nonlinearity. In addition, the amacrine cell signal is low-pass filtered to account for the temporal delay. From the integrated input to the homogeneity detector, we calculated iso-rate and iso-latency curves (Figures 7D and 7E).

Details of the models are provided in [Supplemental Experimental Procedures](#).

SUPPLEMENTAL INFORMATION

Supplemental Information includes one figure and supplemental text and can be found with this article online at [doi:10.1016/j.neuron.2011.10.039](https://doi.org/10.1016/j.neuron.2011.10.039).

ACKNOWLEDGMENTS

We thank A. Borst for comments on the manuscript and the members of the Gollisch Lab for helpful discussions. This work was supported by the Max Planck Society, the German Initiative of Excellence, the International Human Frontier Science Program Organization, the German Ministry for Education and Research through the Bernstein Center for Computational Neuroscience Munich, and the Deutsche Forschungsgemeinschaft (DFG) through the Collaborative Research Center 889.

Accepted: October 14, 2011

Published: January 25, 2012

REFERENCES

- Baccus, S.A., Öveczky, B.P., Manu, M., and Meister, M. (2008). A retinal circuit that computes object motion. *J. Neurosci.* *28*, 6807–6817.
- Bellavance, M.A., Demers, M., and Deschênes, M. (2010). Feedforward inhibition determines the angular tuning of vibrissal responses in the principal trigeminal nucleus. *J. Neurosci.* *30*, 1057–1063.
- Benda, J., Gollisch, T., Machens, C.K., and Herz, A.V. (2007). From response to stimulus: adaptive sampling in sensory physiology. *Curr. Opin. Neurobiol.* *17*, 430–436.
- Burkhardt, D.A., and Fahey, P.K. (1998). Contrast enhancement and distributed encoding by bipolar cells in the retina. *J. Neurophysiol.* *80*, 1070–1081.
- Burkhardt, D.A., Fahey, P.K., and Sikora, M. (1998). Responses of ganglion cells to contrast steps in the light-adapted retina of the tiger salamander. *Vis. Neurosci.* *15*, 219–229.
- Burrone, J., and Lagnado, L. (2000). Synaptic depression and the kinetics of exocytosis in retinal bipolar cells. *J. Neurosci.* *20*, 568–578.
- Cafaro, J., and Rieke, F. (2010). Noise correlations improve response fidelity and stimulus encoding. *Nature* *468*, 964–967.
- Chen, X., Hsueh, H.A., Greenberg, K., and Werblin, F.S. (2010). Three forms of spatial temporal feedforward inhibition are common to different ganglion cell types in rabbit retina. *J. Neurophysiol.* *103*, 2618–2632.
- Chichilnisky, E.J. (2001). A simple white noise analysis of neuronal light responses. *Network* *12*, 199–213.
- Crook, J.D., Peterson, B.B., Packer, O.S., Robinson, F.R., Troy, J.B., and Dacey, D.M. (2008). Y-cell receptive field and collicular projection of parasol ganglion cells in macaque monkey retina. *J. Neurosci.* *28*, 11277–11291.
- Cruikshank, S.J., Lewis, T.J., and Connors, B.W. (2007). Synaptic basis for intense thalamocortical activation of feedforward inhibitory cells in neocortex. *Nat. Neurosci.* *10*, 462–468.
- Demb, J.B., Zghloul, K., Haarsma, L., and Sterling, P. (2001). Bipolar cells contribute to nonlinear spatial summation in the brisk-transient (Y) ganglion cell in mammalian retina. *J. Neurosci.* *21*, 7447–7454.
- Enroth-Cugell, C., and Robson, J.G. (1966). The contrast sensitivity of retinal ganglion cells of the cat. *J. Physiol.* *187*, 517–552.
- Enroth-Cugell, C., and Freeman, A.W. (1987). The receptive-field spatial structure of cat retinal Y cells. *J. Physiol.* *384*, 49–79.
- Gabernet, L., Jadhav, S.P., Feldman, D.E., Carandini, M., and Scanziani, M. (2005). Somatosensory integration controlled by dynamic thalamocortical feed-forward inhibition. *Neuron* *48*, 315–327.
- Geffen, M.N., de Vries, S.E., and Meister, M. (2007). Retinal ganglion cells can rapidly change polarity from Off to On. *PLoS Biol.* *5*, e65.
- Gollisch, T., and Herz, A.M. (2005). Disentangling sub-millisecond processes within an auditory transduction chain. *PLoS Biol.* *3*, e8.
- Gollisch, T., and Meister, M. (2008). Rapid neural coding in the retina with relative spike latencies. *Science* *319*, 1108–1111.
- Gollisch, T., and Meister, M. (2010). Eye smarter than scientists believed: neural computations in circuits of the retina. *Neuron* *65*, 150–164.
- Gollisch, T., Schütze, H., Benda, J., and Herz, A.V. (2002). Energy integration describes sound-intensity coding in an insect auditory system. *J. Neurosci.* *22*, 10434–10448.
- Hochstein, S., and Shapley, R.M. (1976). Linear and nonlinear spatial subunits in Y cat retinal ganglion cells. *J. Physiol.* *262*, 265–284.
- Ishikane, H., Kawana, A., and Tachibana, M. (1999). Short- and long-range synchronous activities in dimming detectors of the frog retina. *Vis. Neurosci.* *16*, 1001–1014.
- Ishikane, H., Gangi, M., Honda, S., and Tachibana, M. (2005). Synchronized retinal oscillations encode essential information for escape behavior in frogs. *Nat. Neurosci.* *8*, 1087–1095.
- Jarsky, T., Cembrowski, M., Logan, S.M., Kath, W.L., Rieke, H., Demb, J.B., and Singer, J.H. (2011). A synaptic mechanism for retinal adaptation to luminance and contrast. *J. Neurosci.* *31*, 11003–11015.
- Mariani, A.P. (1986). Photoreceptors of the larval tiger salamander retina. *Proc. R. Soc. Lond. B Biol. Sci.* *227*, 483–492.
- Masland, R.H. (2001). The fundamental plan of the retina. *Nat. Neurosci.* *4*, 877–886.
- Molnar, A., Hsueh, H.A., Roska, B., and Werblin, F.S. (2009). Crossover inhibition in the retina: circuitry that compensates for nonlinear rectifying synaptic transmission. *J. Comput. Neurosci.* *27*, 569–590.
- Münch, T.A., da Silveira, R.A., Siebert, S., Viney, T.J., Awatramani, G.B., and Roska, B. (2009). Approach sensitivity in the retina processed by a multifunctional neural circuit. *Nat. Neurosci.* *12*, 1308–1316.
- Olshausen, B.A., and Field, D.J. (2005). How close are we to understanding V1? *Neural Comput.* *17*, 1665–1699.
- Öveczky, B.P., Baccus, S.A., and Meister, M. (2003). Segregation of object and background motion in the retina. *Nature* *423*, 401–408.
- Porter, J.T., Johnson, C.K., and Agmon, A. (2001). Diverse types of interneurons generate thalamus-evoked feedforward inhibition in the mouse barrel cortex. *J. Neurosci.* *21*, 2699–2710.
- Pouille, F., and Scanziani, M. (2001). Enforcement of temporal fidelity in pyramidal cells by somatic feed-forward inhibition. *Science* *293*, 1159–1163.
- Pouzat, C., Mazor, O., and Laurent, G. (2002). Using noise signature to optimize spike-sorting and to assess neuronal classification quality. *J. Neurosci. Methods* *122*, 43–57.
- Riesenhuber, M., and Poggio, T. (2000). Models of object recognition. *Nat. Neurosci. Suppl.* *3*, 1199–1204.

- Roska, B., Molnar, A., and Werblin, F.S. (2006). Parallel processing in retinal ganglion cells: how integration of space-time patterns of excitation and inhibition form the spiking output. *J. Neurophysiol.* *95*, 3810–3822.
- Schwartz, G., and Rieke, F. (2011). Perspectives on: information and coding in mammalian sensory physiology: nonlinear spatial encoding by retinal ganglion cells: when $1 + 1 \neq 2$. *J. Gen. Physiol.* *138*, 283–290.
- Segev, R., Puchalla, J., and Berry, M.J., 2nd. (2006). Functional organization of ganglion cells in the salamander retina. *J. Neurophysiol.* *95*, 2277–2292.
- Sestokas, A.K., Lehmkuhle, S., and Kratz, K.E. (1987). Visual latency of ganglion X- and Y-cells: a comparison with geniculate X- and Y-cells. *Vision Res.* *27*, 1399–1408.
- Shapley, R.M., and Victor, J.D. (1979). Nonlinear spatial summation and the contrast gain control of cat retinal ganglion cells. *J. Physiol.* *290*, 141–161.
- Sherry, D.M., Bui, D.D., and Degrip, W.J. (1998). Identification and distribution of photoreceptor subtypes in the neotenic tiger salamander retina. *Vis. Neurosci.* *15*, 1175–1187.
- Singer, J.H., and Diamond, J.S. (2006). Vesicle depletion and synaptic depression at a mammalian ribbon synapse. *J. Neurophysiol.* *95*, 3191–3198.
- Strowbridge, B.W. (2009). Role of cortical feedback in regulating inhibitory microcircuits. *Ann. N Y Acad. Sci.* *1170*, 270–274.
- Sun, Q.Q., Huguenard, J.R., and Prince, D.A. (2006). Barrel cortex microcircuits: thalamocortical feedforward inhibition in spiny stellate cells is mediated by a small number of fast-spiking interneurons. *J. Neurosci.* *26*, 1219–1230.
- Towe, A.L., and Harding, G.W. (1970). Extracellular microelectrode sampling bias. *Exp. Neurol.* *29*, 366–381.
- Victor, J.D. (1988). The dynamics of the cat retinal Y cell subunit. *J. Physiol.* *405*, 289–320.
- Victor, J.D., and Shapley, R.M. (1979). The nonlinear pathway of Y ganglion cells in the cat retina. *J. Gen. Physiol.* *74*, 671–689.
- Werblin, F.S., and Dowling, J.E. (1969). Organization of the retina of the mud-puppy, *Necturus maculosus*. II. Intracellular recording. *J. Neurophysiol.* *32*, 339–355.
- Wu, S.M., Gao, F., and Maple, B.R. (2000). Functional architecture of synapses in the inner retina: segregation of visual signals by stratification of bipolar cell axon terminals. *J. Neurosci.* *20*, 4462–4470.